Available online at www.sciencedirect.com
ScienceDirect
European Journal of Mechanics A/Solids 27 (2008) 285–301

On the crack face boundary conditions in electromechanical fracture and an experimental protocol for determining energy release rates

Wenyuan Li [a], Robert M. McMeeking [b], Chad M. Landis [a,*]

[a] *Department of Aerospace Engineering and Engineering Mechanics, University of Texas at Austin, Austin, TX 78712-0235, USA*
[b] *Department of Mechanical Engineering and Materials Department, University of California, Santa Barbara, CA 93106, USA*

Received 3 May 2007; accepted 31 August 2007

Available online 12 September 2007

Abstract

The fracture mechanics of electromechanical materials has been investigated for well over a decade, yet there still exists controversy over the appropriate crack face boundary conditions for non-conducting cracks. In this paper an experimental protocol for measuring the energy release rate in a non-linear reversible electromechanical body is proposed and summarized. The potential results from the proposed experimental approach are capable of shedding light on the true physical nature of the conditions prevailing at the crack surface and in the space within the crack. The experimental procedure is simulated numerically for a linear piezoelectric specimen in a four point bending configuration subjected to electrical loading perpendicular to the crack. The focus of these investigations is on a comparison between the commonly used exact crack face boundary condition and the recently proposed energetically consistent boundary conditions. To perform the numerical calculation with a wide range of electrical and mechanical loadings, two efficient finite element formulations are presented for the general analysis of crack problems with non-linear crack face boundary conditions. Methods for the numerical determination of the crack tip energy release rate and the simulation of the experimental method for obtaining the total energy release rate are developed. Numerical results for the crack tip and total energy release rate are given for both the exact and energetically consistent boundary conditions. It is shown that the crack tip energy release rate calculated under energetically consistent boundary conditions is equal to the total energy release rate generated from the simulated experimental method. When the exact boundary conditions are used, there is no such agreement.

Keywords: Piezoelectric; Fracture; Finite element method; Non-linear electrical boundary conditions

1. Introduction

Over the past few decades, a rather large literature has developed for the fracture mechanics of linear piezoelectric material, and a review of recent work can be found in McMeeking (1999). As yet, there has been little success in the attempts to correlate experimental data with the predictions of theoretical and computational models for the initiation of crack growth in piezoelectric materials. Only when ad hoc assumptions with little grounding in physics are utilized can models be made to agree with experimental observations. A possible reason for this situation is that the relevance

* Corresponding author. Tel.: +(512) 471 3924; fax: +(512) 471 5500.
E-mail address: landis@mail.utexas.edu (C.M. Landis).

0997-7538/$ – see front matter
doi:10.1016/j.euromechsol.2007.08.007

of the experimental data is uncertain. No fundamental experiments for measuring the energy release rate for cracks in piezoelectric materials have been successfully completed. In principle, the method of compliance calibration, as used for isotropic, linear elastic materials, Anderson (1991), is available. We are aware of only one attempt to provide such data for a piezoelectric material, Schneider (2006), but this effort is as yet incomplete. The experimental difficulties standing in the way of the successful completion of such measurements is considerable. To motivate further work on such experiments, we lay out below the principles upon which the energy release rate may be deduced from tests in which the applied load and the electric potential drop across the specimen are measured as functions of the load point displacement and the charge on the specimen electrodes. These data are then manipulated to obtain the potential energy for the specimen at chosen levels of load and electric potential difference, and upon differencing with respect to crack area, the energy release rate in the piezoelectric specimen at the chosen levels of load and potential difference is obtained. Such an experimental protocol, if it could be completed successfully, would yield unambiguous data for the critical energy release rate for crack propagation in situations where various combinations of mechanical load and electric field are being applied.

Another reason for the failure to achieve consistency between experimental data and theoretical and computational fracture mechanics simulations for piezoelectric materials is the primitive nature of the models so far utilized. In attempts to remedy this situation, the simulations have been extended to try to bring more realistic features into the fracture mechanics. For example, different models of the electrical boundary conditions on the crack surfaces have been proposed based on differing assumptions about the electrical characteristics of the medium within the crack gap, Parton (1976), Deeg (1980), Pak (1992), Suo et al. (1992), Hao and Shen (1994), Dunn (1994), McMeeking (2004), and Landis (2004). Within a linearized analysis of material behavior, the "exact" crack model by Hao and Shen (1994) represents the most ambitious attempt at physical consistency. In this model, the crack gap is treated as a capacitor and the electric field between the faces is thus dependent on the crack opening displacement and the electric potential in the adjacent material. In contrast, the permeable, Parton (1976), and impermeable models, Deeg (1980), Pak (1992) and Suo et al. (1992), of the crack are more simplistic. In the former, the crack is assumed to cause no perturbation to the electric field, whereas the electric field cannot penetrate the crack at all in the latter case. All three of these crack models assume that the crack faces are traction free.

The permeable and impermeable models have obvious deficiencies in regard to representing the interaction of the electric field and the crack. Furthermore, there are no experimental data that confirm the utility of these models as the basis of fracture mechanics for piezoelectric materials. On the other hand, the exact model would seem to provide a more realistic approach to modeling the electrical behavior of cracks, albeit at the expense of non-linear features that are introduced into the analysis. However, a discrepancy was found between the total and the crack tip energy release rates by McMeeking (2004), when he investigated these for a Griffith crack having the exact crack face boundary conditions in a piezoelectric material. The crack tip energy release rate is that calculated as the flux of mechanical and electrical energy to an extending crack tip, whereas the total energy release rate is the rate at which the potential energy of the systems falls as the crack extends. These two concepts should yield the same value in any conservative system, such as that represented by a brittle piezoelectric material with a crack. Recently, this discrepancy was repaired by Landis (2004) through the implementation of energetically consistent boundary conditions, where the electrically "exact" boundary condition is augmented by a traction on flaw faces tending to close the crack. When such boundary conditions are imposed in the problems solved by Landis (2004), the total and crack tip energy release rates are identical.

An additional phenomenon that is thought to occur within the crack in a piezoelectric material is electrical discharge. Since the dielectric constant of technologically important piezoelectric materials is typically very high (of the order 10^3), the electric field within the crack can be very high even if the potential difference across the specimen is modest. In many cases, the predicted electric field within the crack is much higher than the known breakdown strength of air. As a consequence, it must be assumed that electrical discharge takes place within the crack, and this effect should be accounted for in simulations of cracks in piezoelectric specimens subject to electric loading.

The primary objective of this paper is to present an experimental protocol for measuring the energy release rate in a cracked electromechanically coupled solid. Thereafter, this protocol is simulated numerically using the finite element method to analyze a cracked, linear, piezoelectric beam subjected to four-point bending, with an electric field applied perpendicular to the flaw. Four different types of boundary conditions are applied on the surfaces of the crack; *permeable, impermeable, "exact" and energetically consistent*. The energy release rate and crack tip intensity factors are then computed when the beam is under various combinations of applied load and electric field. Results for the

energy release rates predicted from each of the boundary conditions are interpreted and discussed in relation to the experimental protocol. It is demonstrated that an unacceptable inconsistency in the total and crack tip energy release rates exists when the conventional "exact" boundary conditions are applied on the crack surfaces. Finally, the effects of electrical discharge on the energy release rate are modeled and shown to significantly reduce the influence of the applied electric field. Since electrical discharge is essentially inevitable within the flaw gap when realistic electric fields are applied to the cracked component, this last result is of considerable importance.

2. An experimental protocol for determining the energy release rate in cracked electromechanical bodies

Consider a crack of area A in a body with non-linear but reversible electromechanically coupled constitutive response. The body is contained in another non-linear dielectric medium, whose properties include the possibility of electric breakdown, e.g. air, vacuum, or an electrically inert liquid. The arguments presented here can also be rigorously applied to irreversible behavior as long as no non-proportional loading has occurred at any point in the body. For the sake of simplicity in the presentation we assume that the mechanical loading is characterized by a point load P and a displacement of the load point Δ. Similarly, the electrical loading is characterized by an electric potential drop of magnitude V between two electrodes and the total charge of magnitude Q that resides on those electrodes. The energy that is stored in the system U, including both the cracked body and its surroundings, is given by

$$U = \int_{\Delta_0}^{\Delta} P(\Delta', Q')\, d\Delta' + \int_{Q_0}^{Q} V(\Delta', Q')\, dQ'. \tag{2.1}$$

Here Δ_0 and Q_0 are the initial or reference load point displacement and electrode charge. It follows from Eq. (2.1) and the path independence of these integrals implied by reversibility that the force P and the voltage V can be obtained from the stored energy as

$$P = \frac{\partial U}{\partial \Delta} \quad \text{and} \quad V = \frac{\partial U}{\partial Q}. \tag{2.2}$$

Then, accounting for the work done by the electrical and mechanical loads, the total potential energy of the system Π is

$$\Pi = U - P\Delta - VQ. \tag{2.3}$$

The reduction in the potential energy per increase in the crack area is defined as the energy release rate (see for example Anderson, 1991), such that

$$\mathcal{G} = -\frac{d\Pi}{dA} \tag{2.4}$$

Eqs. (2.1)–(2.4) can be used as the basis for an experimental determination of the energy release rate for a cracked electromechanical body and its surroundings. This is accomplished by comparing the electromechanical response of two samples that differ by a slight amount in their crack area, see Fig. 1. For a plane specimen, which characterizes most experimentally significant geometries, the change in crack area dA is, of course, directly related to the change in crack length, given uniform growth of the crack. The two different cracked bodies are loaded to the same electromechanical level, characterized by any combination of load/displacement and voltage/charge. Eq. (2.4) can then be used to compute the energy release rate from the following difference equation

$$\mathcal{G} = \frac{\Pi(A) - \Pi(A + dA)}{dA}. \tag{2.5}$$

The choice of whether to keep the load, voltage, displacement or charge constant or let them vary, is arbitrary, consistent with the constraints of the governing equations. Differences in the resulting value of $\mathcal{G}$ arising among the various choices will be second order in dA. The resulting procedure for computing $\mathcal{G}$ is illustrated schematically in Fig. 2. Let us assume that the load-displacement and voltage–charge plot for the specimen illustrated in Fig. 1 are given in Fig. 2. The upper P–Δ curve and lower V–Q curve correspond to the crack area A, and the other two curves correspond to the crack area $A + dA$. The dashed lines correspond to holding the load and the charge constant during

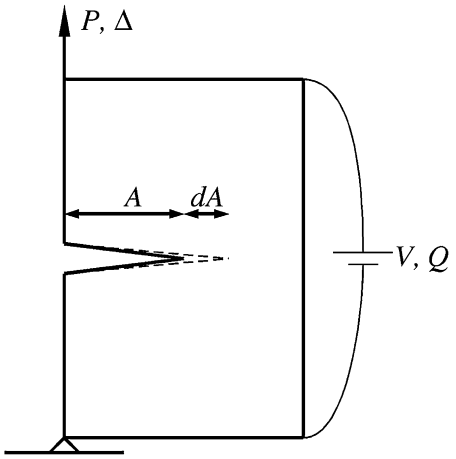

Fig. 1. A schematic of a cracked body with mechanical loading by a force P and load point displacement Δ, and electrical loading by a voltage drop V and electrode charge Q.

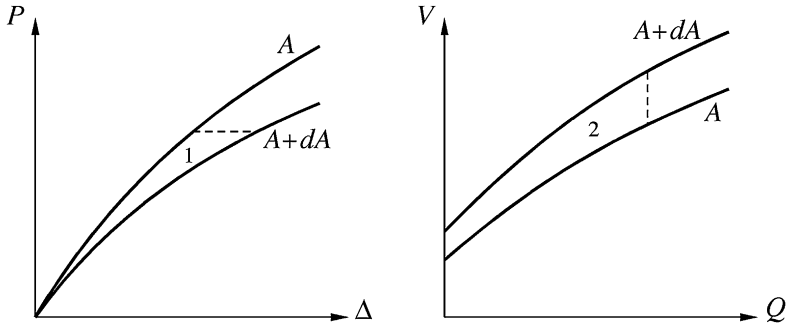

Fig. 2. A schematic of the load-deflection and voltage–charge curves for samples with different crack areas A and $A + dA$. The mechanical load is applied first holding the charge fixed at zero, then the electrical load is applied holding the load fixed. The approximation to the energy release rate for this loading scenario is then $\mathcal{G} \approx (\text{Area } 1 - \text{Area } 2)/dA$.

the calculation of the energy release rate. The estimate for the energy release rate at a crack length of $A + dA/2$ is simply the area 1 minus area 2 divided by dA.

The protocol just described can be implemented experimentally or computationally. The barriers to experimental implementation are formidable, but will not be discussed here. In the following sections we will implement the procedure just described computationally on a linear piezoelectric four-point bend specimen. The purpose of these studies will be to investigate the accuracy of the proposed procedure, and to characterize numerically the effects of several different types of boundary conditions used to model the electrical conditions on the crack surface. In what follows, we will designate as the "experimental procedure" the numerical implementation of the protocol for obtaining the energy release rate that we have just described.

3. Fundamentals of linear piezoelectricity

Prior to presentation of the specific geometry that we intend to investigate, some theoretical preliminaries associated with the fracture mechanics of linear piezoelectric bodies will be discussed. For a linear piezoelectric material, the equations governing a small deformation, small electric field, electrically and mechanically quasi-static, isothermal boundary value problem for this solid will be reviewed in this section. Assume the volume of material is V and the boundary surface is S. The mechanical equilibrium equations are given by

$$\sigma_{ji,j} + b_i = 0 \quad \text{and} \quad \sigma_{ij} = \sigma_{ji} \quad \text{in } V, \tag{3.1}$$

$$\sigma_{ji} n_j = t_i \quad \text{on } S. \tag{3.2}$$

Here σ_{ij} represents the symmetric Cauchy stress tensor, b_i represents the body force per unit volume, n_i represents the unit vector normal to the surface pointing from the volume, and t_i represents the surface traction. In this section, summation is implied over repeated indices, and $_{,i}$ is the partial differentiation with respect to the x_i direction.

The infinitesimal strain tensor ε_{ij} is linked to mechanical displacement components u_i as

$$\varepsilon_{ij} = \frac{1}{2}(u_{i,j} + u_{j,i}). \tag{3.3}$$

The electric displacement D_i is related to the free charge per unit volume q and the charge per unit area external to the body ω through Gauss's law as

$$D_{i,i} = q \quad \text{in } V, \tag{3.4}$$

$$D_i n_i = -\omega \quad \text{on } S. \tag{3.5}$$

Under quasi-static conditions, the electric field components E_i can be written as the gradient of the electric potential ϕ as

$$E_i = -\phi_{,i}. \tag{3.6}$$

For conservative materials, an electrical enthalphy density h, which is a functional of the strain and electric field, can be defined as

$$h = \hat{u} - E_i D_i. \tag{3.7}$$

Here $\hat{u}$ is the internal energy density, defined by

$$\hat{u} = \int_{\varepsilon_{ij}^r}^{\varepsilon_{ij}} \sigma_{ij}\, d\varepsilon'_{ij} + \int_{P_k^r}^{D_k} E_k\, dD'_k. \tag{3.8}$$

The lower limits on the integrals in (3.8) are the remanent strain ε_{ij}^r and remanent polarization P_i^r, which are assumed to be frozen within the material. The electrical enthalpy is introduced because it is used with the scalar potential finite element formulation and in the most useful definition of the electromechanical form of the J-integral, which can be used as a method for calculating the energy release rate.

Finally, the linear piezoelectric constitutive law relating the four electromechanical field quantities can be given in four different combinations. Two of these forms relevant to this work are given as,

$$\sigma_{ij} = c_{ijkl}^E(\varepsilon_{kl} - \varepsilon_{kl}^r) - e_{kij}E_k, \qquad D_i - P_i^r = e_{ikl}(\varepsilon_{kl} - \varepsilon_{kl}^r) + \kappa_{ij}^\varepsilon E_j \tag{3.9}$$

and

$$\sigma_{ij} = c_{ijkl}^D(\varepsilon_{kl} - \varepsilon_{kl}^r) - h_{kij}(D_k - P_k^r), \qquad E_i = -h_{ikl}(\varepsilon_{kl} - \varepsilon_{kl}^r) + \beta_{ij}^\varepsilon(D_j - P_j^r). \tag{3.10}$$

Here c_{ijkl}^E and c_{ijkl}^D are fourth rank tensors of elasticity, e_{kij} and h_{kij} are third rank tensors of piezoelectricity, and κ_{ij}^ε and β_{ij}^ε are second rank dielectric tensors.

Eqs. (3.1)–(3.6) can also be stated in the following two weak forms as

$$\int_V \sigma_{ij}\delta\varepsilon_{ij} - D_i\delta E_i\, dV = \int_V b_i\delta u_i - q\delta\phi\, dV + \int_S t_i\delta u_i - \omega\delta\phi\, dS \tag{3.11}$$

or

$$\int_V \sigma_{ij}\delta\varepsilon_{ij} + E_i\delta D_i\, dV = \int_V b_i\delta u_i + \phi\delta q\, dV + \int_S t_i\delta u_i + \phi\delta\omega\, dS. \tag{3.12}$$

Eq. (3.11) is the foundation for a scalar potential finite element formulation that implements the electric potential ϕ as nodal degrees of freedom. For such a formulation the variational quantities $\delta\varepsilon_{ij}$ and δE_i must satisfy Eqs. (3.3) and (3.6), and then the constitutive equations (3.9) are applied, Allik and Hughes (1970). For boundary value problems with body charge $q = 0$, the variational quantities δD_i and $\delta\omega$ must satisfy $\delta D_i = \epsilon_{ijk}\delta\psi_{j,k}$ and $\delta\omega = -\epsilon_{ijk}n_i\delta\psi_{j,k}$, where ϵ_{ijk} is the permutation tensor. For the vector potential formulation the constitutive form of Eq. (3.10) is required. Then, Eq. (3.12) leads to the vector potential finite element formulation, which uses the vector potential components ψ_i as nodal degrees of freedom, Landis (2002).

4. Boundary conditions

When a linear piezoelectric boundary value problem is solved, it is of course necessary to specify both mechanical and electrical boundary conditions on all bounding surfaces. Here we will first discuss the conditions which are commonly used to model non-crack face surfaces and then we will move on to the more interesting crack face boundary conditions. For non-crack face surfaces, within linear piezoelectric theory, no distinction is made between the deformed or undeformed configuration of the body, and hence complications associated with tractions due to Maxwell stresses do not arise. The mechanical boundary conditions on such surfaces effectively reduce to known applied tractions or known applied displacements. On surfaces with attached electrodes, the electrical boundary condition is that the electric potential is fixed and constant over any part of the surface connected to the same electrode. On surfaces without electrodes the electrical boundary conditions are not as clear. Since the air/fluid surrounding any specimen has dielectric properties, energy and electrical fields can be transmitted across the specimen boundaries. To account for this physical behavior, a solution for the electric fields in all of the surrounding space is required. Such solutions can be obtained using boundary elements or a Dirichlet to Neumann map on the surface of the geometry. However, such complete solutions are rarely carried out. Standard practice recognizes that the dielectric constants of most piezoelectric materials of technological interest are 100–1000 times larger than that of free space, and hence it is usually assumed that it is valid to take the limit that the dielectric constant of the surrounding medium is zero. This approximation at non-electroded boundaries forces the normal component of the electric displacement to vanish at the boundary. Hence, the usual electrical boundary conditions are that either the potential ϕ is specified, or the normal component of electric displacement $D_n = D_i n_i$ is taken to be zero.

As discussed in the introduction, several different modeling approaches for the boundary conditions on crack faces have appeared in the literature. These boundary conditions and the rationale behind them will be presented and discussed in the following sub-sections.

4.1. Permeable boundary conditions

The permeable boundary conditions were first proposed by Parton (1976). This model for the crack recognizes that within the assumptions of linear piezoelectricity there is no distinction between the deformed and undeformed configurations of the material. In the undeformed configuration the crack faces are closed, and in such a situation the electrical fields will distribute themselves as if the crack did not exist. The mathematical statements that describe these electrical conditions are that electric potential and the normal component of the electric displacement are continuous across the crack, i.e.

$$\phi^+ = \phi^- \quad \text{and} \quad D_n^+ = D_n^-. \tag{4.1}$$

Here the superscripts $+$ and $-$ denote the top and bottom crack faces. It should be obvious that the physical arguments used to justify the permeable boundary conditions are weak because, upon loading, the crack will open and the medium that fills the crack gap will be able to support an electrical potential drop across the opening. This effect is amplified by the high dielectric constants of technologically important piezoelectric materials, which leads to electric fields within the crack that are orders of magnitude larger than that in the material.

4.2. Impermeable boundary conditions

The impermeable boundary condition model, proposed by Deeg (1980), was introduced to address the fact that fracture generally occurs when cracks are open. The same argument used to justify the charge free boundary conditions on non-crack face surfaces is used to motivate the impermeable crack face boundary conditions. Due to the fact that the permittivity of the medium within the crack gap is usually much lower than that of the solid body, it is assumed that the permittivity of the crack gap can be approximated as zero. This assumption then implies that the normal component of electric displacement on both crack faces are zero, i.e.

$$D_n^+ = D_n^- = 0. \tag{4.2}$$

The obvious physical question that arises for the impermeable boundary conditions is, how does the assumption of a zero permittivity crack gap affect solutions? To address this question the two following models allow the electric field

to permeate the crack gap. Later we will investigate the differences in the solutions that arise from the permeable and impermeable boundary conditions, along with two additional types of boundary conditions that attempt to improve upon these two simple approaches.

4.3. "Exact" or semi-permeable boundary conditions

In order to address the facts that cracks are actually open and that electrical fields can permeate the crack gap, Hao and Shen (1994) introduced electrical boundary conditions that treat the crack faces as an aggregate of parallel plate capacitors. In the literature these boundary conditions have been referred to as "exact", semi-permeable, or Hao and Shen boundary conditions. These conditions assume that the crack gap behaves like a linear dielectric material with permittivity κ_0 and that the electric field and electric displacement within the crack gap are normal to the crack surfaces. Mathematically these conditions are stated as

$$D_n^+ = D_n^- = D_c, \tag{4.3}$$

$$D_c = \kappa_0 E_c = -\kappa_0 \frac{\phi^+ - \phi^-}{u_n^+ - u_n^-} = -\kappa_0 \frac{\Delta\phi}{\Delta u_n}. \tag{4.4}$$

Here D_c is the normal component of electric displacement supported by the crack gap, E_c is the electric field in the crack gap, $\Delta\phi$ is the potential drop across the crack gap, Δu_n is the crack opening displacement, the subscript n represents the component normal to the crack faces, and κ_0 is the linear dielectric permittivity of the gap, which is usually identified with the permittivity of free space 8.854×10^{-12} C/V m.

In addition to the stated electrical conditions, each of the crack face boundary conditions in Subsections 4.1–4.3 also assume that the crack faces are mechanically traction free. Numerous works have focused on the "exact" electrical boundary condition along with traction free mechanical boundary conditions. These boundary conditions appear to be physically sound and justifiable. However, McMeeking (2004) has pointed out that there is a discrepancy between the total energy release rate and the crack tip energy release rate for a Griffith crack configuration with this combination of electrical and mechanical boundary conditions. The fundamental reason for this discrepancy is that, when charged, capacitor plates are drawn towards one another because there is a force between them. Hence, if the crack gap can store energy, then the crack faces are in general not traction free.

4.4. Energetically consistent boundary conditions

In order to repair the inconsistency identified by McMeeking (2004), Landis (2004) proposed energetically consistent boundary conditions, with an electrical component very similar to the "exact" boundary conditions plus an additional closing traction on crack faces. The basic idea of the model is to assign an energy, specifically an electrical enthalpy h_c, to the crack gap, and then the variation of this enthalpy with respect to the crack opening displacement is a traction, and the variation with respect to the potential drop is a charge. The energetically consistent crack face boundary conditions for a crack gap are given as

$$\omega^+ = -D_i n_i^+ = D_c = -\frac{dh_c}{dE_c} \quad \text{on } S_c^+, \tag{4.5}$$

$$\omega^- = -D_i n_i^- = -D_c = \frac{dh_c}{dE_c} \quad \text{on } S_c^-, \tag{4.6}$$

$$t_i^+ = \sigma_{ji} n_j^+ = \sigma_c n_i^+ = (h_c + E_c D_c) n_i^+ \quad \text{on } S_c^+, \tag{4.7}$$

$$t_i^- = \sigma_{ji} n_j^- = \sigma_c n_i^- = (h_c + E_c D_c) n_i^- \quad \text{on } S_c^- \tag{4.8}$$

where

$$E_c = -\frac{\phi^+ - \phi^-}{u_n^+ - u_n^-} = -\frac{\Delta\phi}{\Delta u_n}. \tag{4.9}$$

Here, S_c^+ and S_c^- are the top and bottom crack surfaces; ω^+ and ω^- are the surface charge density applied to these crack surfaces, t_i^+ and t_i^- are the surface tractions applied to the crack surfaces, n_i^+ and n_i^- are the unit normal along the top and bottom crack faces pointing away from the solid material, h_c is the electrical enthalpy density of the crack

gap, which depends only on E_c such that $h_c = h_c(E_c)$, and σ_c is the effective stress within the crack gap such that $\sigma_c = h_c + E_c D_c$.

In general the electrical enthalpy can be non-linear and is intended to model the electrical response of the crack gap. A specific form for the energetically consistent boundary conditions that can be used to model the linear response of the gap at low electric field levels, and the non-linear response that occurs during electrical discharge is presented next. If the dielectric constant of the medium within the crack gap is much lower than that of the material body, then high electric fields are generated within the crack gap. Ultimately high electric fields within the crack gap can lead to electrical breakdown, usually in the form of a corona discharge. Following Landis (2004), a simple idealized phenomenological model is proposed with a critical electrical discharge level E_d, such that the crack gap behaves in a linear dielectric manner when electric field within crack gap is below this critical value. Beyond the critical point, the crack gap cannot support electric field larger than E_d, and charge will flow between the crack surfaces such that the electric field remains at this bounding value. Mathematically the model is stated as

$$h_c = -\frac{1}{2}\kappa_0 E_c^2, \quad D_c = \kappa_0 E_c, \quad \sigma_c = \frac{1}{2}\kappa_0 E_c^2 \quad \text{if } |D_c| \leqslant \kappa_0 E_d, \tag{4.10}$$

$$h_c = -\frac{1}{2}\kappa_0 E_d^2, \qquad D_c = \operatorname{sgn}(\omega_d)\kappa_0 E_d + \omega_d, \tag{4.11}$$

$$E_c = \operatorname{sgn}(\omega_d) E_d, \quad \sigma_c = E_d|\omega_d| + \frac{1}{2}\kappa_0 E_d^2 \quad \text{if } |D_c| \geqslant \kappa_0 E_d. \tag{4.12}$$

Here, ω_d represents the amount of charge per unit area transferred between the crack faces. Note that in some of the computations described below, the breakdown strength of the medium in the crack gap is taken to be infinite, so that unlimited linear permeation of the electric field occurs into the space in the flaw.

5. Calculation of fracture parameters

Several authors have investigated the effects of different crack face boundary conditions using the idealized geometry of a center crack in an infinite two-dimensional linear piezoelectric medium, e.g. Dunn (1994), McMeeking (2004), and Landis (2004). Even with the non-linearities associated with the "exact" and energetically consistent boundary conditions, this model requires only the solution of a quadratic or cubic algebraic equation. For geometries relevant to experimental measurements, analytic solutions of this type are not attainable and numerical methods are required for the model analysis. Appendix A discusses two useful finite element formulations for studying piezoelectric fracture problems on general geometries, along with model reduction techniques that allow for relatively rapid solutions of the non-linear boundary conditions. Once a given finite element solution is in hand, we are interested in obtaining several relevant fracture parameters, including stress and electric displacement intensity factors and the energy release rates. Where the energy release rate is computed based on the fields local to the crack tip, such a quantity will be referred to as the crack tip energy release rate $\mathcal{G}_{\text{tip}}$. Since the "exact" boundary conditions yield different results for the energy release rates we will make a distinction between $\mathcal{G}$ and $\mathcal{G}_{\text{tip}}$ based on the method of calculation.

5.1. Numerical calculation of $\mathcal{G}_{\text{tip}}$ using K_{I} and K_{D}

Consider a crack in a linear piezoelectric body under mixed Mode I and Mode D (also called Mode IV) loading. The crack tip energy release rate can be given in terms of the intensity factors as

$$\mathcal{G}_{\text{tip}} = H_{11} K_{\text{I}}^2 + 2H_{12} K_{\text{I}} K_{\text{D}} + H_{22} K_{\text{D}}^2. \tag{5.1}$$

Here H_{11}, H_{12} and H_{22} are components of the Irwin matrix, which depend only on the material properties of the piezoelectric solid. The stress and electric displacement intensity factors characterize the near tip electromechanical fields and are defined such that on the plane directly ahead of the crack tip

$$\sigma_{yy} = \frac{K_{\text{I}}}{\sqrt{2\pi r}} \quad \text{and} \quad D_y = \frac{K_{\text{D}}}{\sqrt{2\pi r}} \quad \text{for } \theta = 0. \tag{5.2}$$

Near the crack tip, the crack opening displacement and electric potential drop are given as

$$\begin{Bmatrix} \Delta u_y \\ \Delta\phi \end{Bmatrix} = 4\sqrt{\frac{2r}{\pi}} \begin{bmatrix} H_{11} & H_{12} \\ H_{12} & H_{22} \end{bmatrix} \begin{Bmatrix} K_{\text{I}} \\ K_{\text{D}} \end{Bmatrix}. \tag{5.3}$$

The normal component of the electric displacement can be written as

$$D_y = -\frac{\partial \psi}{\partial x}. \tag{5.4}$$

Where, for the two-dimensional problems considered here, ψ is the z-component of the vector potential. Eqs. (5.2) and (5.4) then imply that

$$K_{\mathrm{D}} = -(\psi - \psi_0)\sqrt{\frac{\pi}{2r}} \tag{5.5}$$

where ψ_0 is the value of the vector potential at the crack tip and ψ is a value of the vector potential on the plane $\theta = 0$ at a distance r from the crack tip.

For the scalar potential formulation, the values of the crack opening and potential drop are computed as nodal quantities at every node along the crack face. Then for any distance r behind the crack tip, Δu_y and $\Delta\phi$ are known and the intensity factors K_{I} and K_{D} can be computed by inverting equation (5.3). For two nodes sufficiently close to the crack tip this procedure should yield similar results for K_{I} and K_{D} and any differences can be used as a measure of the error in the procedure.

For the vector potential formulation, the opening displacement and vector potential ψ are computed from the finite element solution at each crack face node. From ψ, Eq. (5.5) offers a direct method for calculating K_{D}, and then K_{I} can be calculated using Eq. (5.3) as

$$K_{\mathrm{I}} = \left(\frac{1}{4}\sqrt{\frac{\pi}{2r}}\Delta u_y - H_{12}K_{\mathrm{D}}\right)/H_{11}. \tag{5.6}$$

Finally, the crack tip energy release rate can be calculated from (5.1).

We note that there exist more accurate techniques for the numerical determination of the energy release rate, e.g the computation of the electromechanical form of the J-integral, Landis (2004), using the domain integral technique, Li et al. (1985), or the virtual crack extension method, Parks (1974). In fact, the domain integral technique has been used to check the accuracy of the method described above, Li (2006), and the agreement between these two methods is excellent. For example, for the results to be presented later in Fig. 8, the domain integral technique and the method described above differ by less than 1% over the entire range of applied electric fields, except when the magnitude of the energy release rate is very close to zero (on the order of 10^{-5} J/m^2). However, the goal of this work is not to present a more accurate method for the numerical analysis of the energy release rate, but rather to (a) present and model the proposed experimental protocol for the measurement of the energy release rate, and (b) to further demonstrate the inconsistencies associated with the "exact" boundary conditions.

6. The four point bend specimen

Consider a linear piezoelectric four-point bend specimen as illustrated in Fig. 3. Plane strain conditions will be assumed and the material properties, characteristic of PIC-151, are given in Appendix B. For all of the boundary condition types modeled, it can be assumed that the material is poled, as long as it is also assumed that charge separation occurs as new crack faces are formed such that the remanent polarization is perfectly balanced on these new surfaces. This assumption is implicit to the vast majority of fracture mechanics studies on piezoelectric materials. Furthermore, the incorporation of arbitrary levels of charge separation is not difficult, see Landis (2004) and Haug and McMeeking (2006), but is not carried out here for the sake of brevity.

Due to the symmetry of the specimen geometry and the symmetry of the electromechanical loading, only the right half of the beam needs to be analyzed. Fig. 4 illustrates the details of the finite element mesh that has been used to compute the results. Over most of the body, standard eight-noded quadrilateral elements are used. Near the crack tip region, the mesh is refined and the elements attached to the crack tip are standard quarter-point singularity elements.

The first sets of results to be presented are for the two types of linear boundary conditions, permeable and impermeable. For these boundary conditions the stress and electric displacement intensity factors can be given in terms of the four calibration functions M, N, S and T as

$$K_{\mathrm{I}} = \sigma\sqrt{\pi a}\left(1 - \frac{a}{b}\right)^{-3/2} M\left(\frac{a}{b}\right) + \frac{H_{12}}{H_{11}} D\sqrt{\pi a}\left(1 - \frac{a}{b}\right)^{-3/2} N\left(\frac{a}{b}\right), \tag{6.1}$$

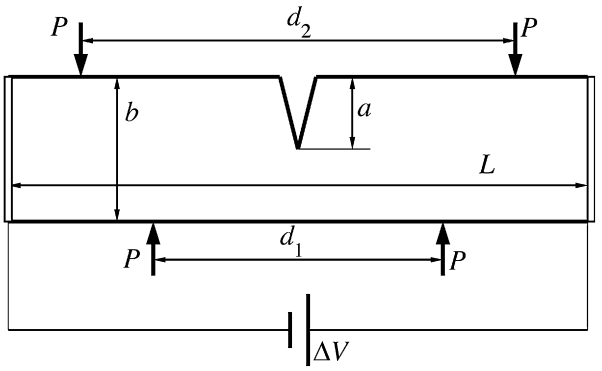

Fig. 3. The geometry of the four-point bend specimen. The actual geometry analyzed has dimensions, $d_1 = 10$ mm, $d_2 = 20$ mm, $L = 28$ mm, $b = 4$ mm and $a = 0.5$–3.5 mm.

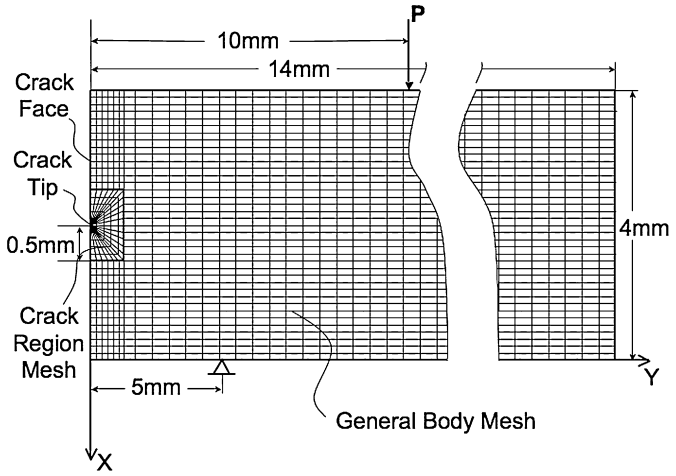

Fig. 4. The schematic of the finite element meshing of the specimen. Eight-noded elements are used with quarter-point elements at the crack tip. Around the crack tip the mesh is refined.

$$K_{\mathrm{D}} = -\frac{H_{12}}{H_{22}}\sigma\sqrt{\pi a}\left(1-\frac{a}{b}\right)^{-3/2} S\left(\frac{a}{b}\right) + D\sqrt{\pi a}\left(1-\frac{a}{b}\right)^{-3/2} T\left(\frac{a}{b}\right) \tag{6.2}$$

where

$$\sigma = \frac{6M}{tb^2} = \frac{3P(d_2-d_1)}{tb^2} \quad \text{and} \quad D = \kappa_{33}^{\sigma} E = -\kappa_{33}^{\sigma}\frac{\Delta V}{L}. \tag{6.3}$$

Note that $N(a/b) = T(a/b) = 0$ and $S(a/b) = M(a/b)$ for the permeable case. Figs. 5(a)–(b) present the dimensionless functions M, N, S and T associated with the stress and electric displacement intensity factors in Eqs. (6.1) and (6.2) for the four-point bend specimen illustrated in Fig. 3. Also included on these figures are thin black and dashed black lines representing the dimensionless functions M and T for the analogous isotropic elastic and isotropic dielectric specimens respectively. Using K_{I} andK_{D}, the energy release rate, either total or crack tip, can be computed using Eq. (5.1).

Next we investigate the effects of the two non-linear boundary condition types, energetically consistent and "exact", on the fracture parameters for the four-point bend specimen. For the "exact" and energetically consistent boundary conditions, the crack gap is assumed to behave in a linear dielectric manner such that electrical discharge is not allowed to occur. Figs. 6(a)–(b) plot K_{I} and K_{D} as functions of the applied electric field, $E = -\Delta V/L$, for a mechanical loading of 2000 N and a crack length of 1 mm for the four different crack face boundary condition types.

Of considerable interest is the fact that the permeable, impermeable and "exact" boundary conditions yield very similar results for K_{I} that are relatively *independent* of the level of the applied electric field. However, the energetically

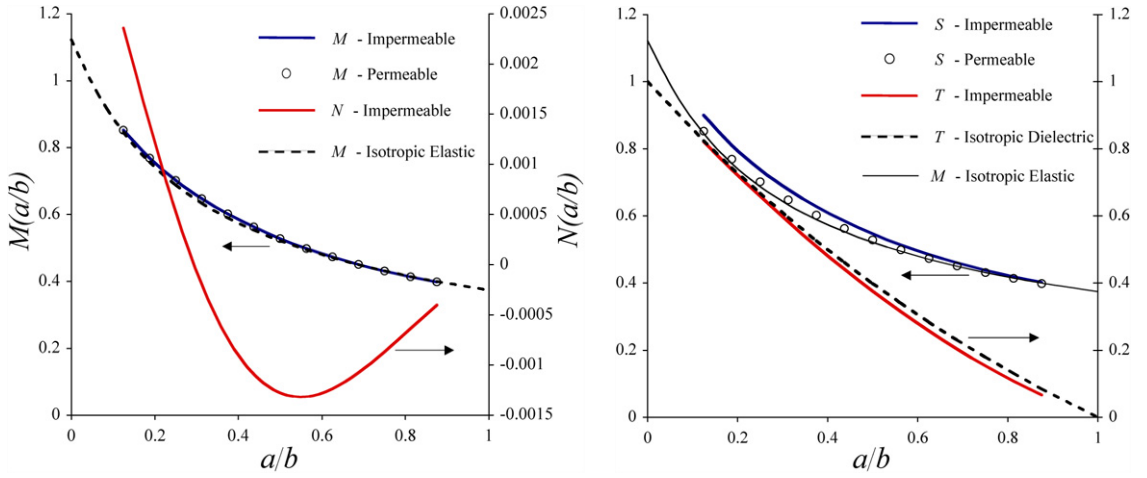

Fig. 5. The dimensionless functions for the stress and electric displacement intensity factors as defined in Eqs. (6.1) and (6.2). Note that *S(a/b)* is equal to $M(a/b)$ for the permeable boundary conditions. Also, both $N(a/b)$ and $T(a/b)$ are equal to zero for the permeable boundary conditions.

consistent boundary conditions predict a distinct dependence of the stress intensity factor on the applied electric field. Given that the electrical boundary conditions are very similar for the energetically consistent and the "exact" boundary conditions, it becomes apparent that the additional mechanical crack face traction associated with the energetically consistent boundary conditions, Eqs. (4.7) and (4.8), is responsible for this dependence of K_{I} on the applied electric field. Fig. 6(b) illustrates the dependence of K_{D} on the applied electric field, with K_{D} being constant for the permeable boundary conditions and linearly dependent on the applied electric field for the impermeable crack face boundary conditions. The effects of the crack gap's ability to support electric fields can be ascertained by comparing the results for the "exact" and energetically consistent boundary conditions to those for the impermeable boundary conditions. Furthermore, the effects of the crack face traction associated with the energetically consistent boundary conditions are particularly apparent for positive levels of electric field, where the results for the "exact" and energetically consistent boundary conditions diverge.

While the results for K_{I} and K_{D} are of interest, they are only useful within a fracture criterion in conjunction with an energetic constraint. Specifically, unless the fracture process itself can *supply* energy to the surrounding material, crack growth can only occur if the amount of energy entering the crack tip is positive. Hence, when the fracture process consumes energy, the fracture criterion must at the very least require the inequality $\mathcal{G}_{\mathrm{tip}} > 0$. Fig. 7 plots the energy release rates as a function of the applied electric field for the same set of mechanical loading as in Figs. 6(a)–(b), but for a crack length of 0.75 mm. For each of the boundary condition types the solid lines represent the crack tip energy release rate as computed from Eq. (5.1), and the dots represent the "total" or "global" energy release rate as computed from Eq. (2.5) using a Δa of 0.5 mm. We note that when there is no dissipation in either the material or its surroundings there can be no difference between these two measures of energy release rate. Hence, any difference that does arise represents a failure of the modeling procedure to generate physically consistent results. The results shown on Fig. 7 demonstrate that of the four crack face boundary condition types, only the "exact" boundary conditions generate a significant difference (i.e. not due to the discretization error associated with Eq. (2.5)) between the crack tip and total energy release rates. Furthermore, the crack tip energy release rate for the "exact" boundary conditions is significantly greater than the total energy release rate. Also, the total energy release rate from the "exact" boundary conditions is similar (but always less than) the energy release rate for the energetically consistent boundary conditions. This observation leads to the conclusion that the total energy release rate from the "exact" boundary conditions is a reasonable approximation for the energy release rate for the energetically consistent boundary conditions. Similar observations and conclusions have been made by Landis (2004) from the analysis of the center-cracked plate problem.

In addition to the approximations used to model the crack face boundary conditions, it is also useful to note the approximations applied to the constitutive model for linear piezoelectric materials, Eqs. (3.9) and (3.10). Most piezoelectric materials of technological interest are poled ferroelectric materials. Hence, the constitutive equations

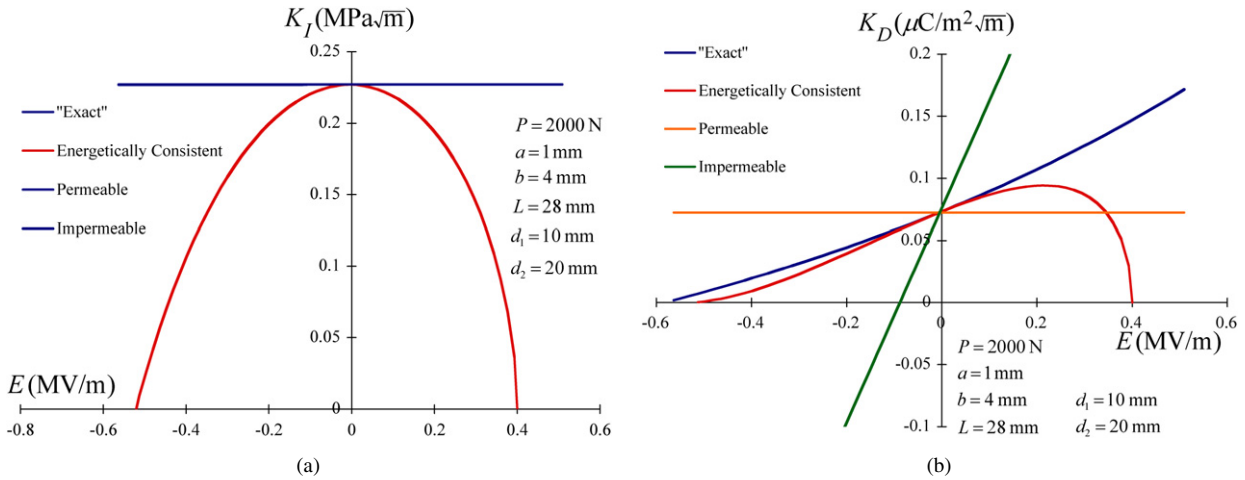

Fig. 6. (a) Stress and (b) electric displacement intensity factors for the four boundary condition types for a given mechanical load as a function of the applied electric field. Note that the "exact", permeable and impermeable lines are indistinguishable from one another in (a), and are plotted with the same color (for colors see the web version of the article).

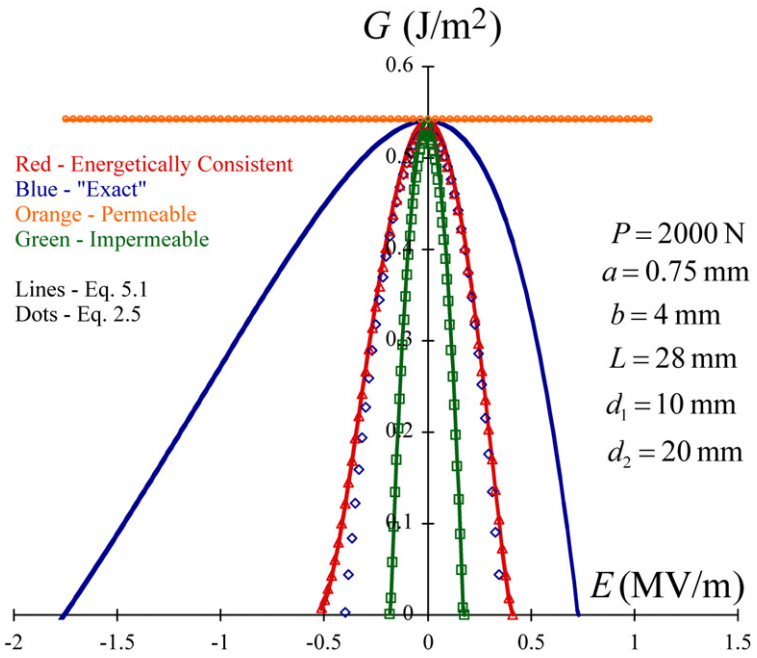

Fig. 7. The energy release rates for the four different boundary condition types for a given mechanical loading of 2000 N as a function of electric field. Solid lines represent the results as computed from Eq. (5.1) and the dots are results computed from Eq. (2.5) using a Δa of 0.5 mm.

(3.9) and (3.10) are valid for the *changes* of strain and polarization with respect to the remanently poled state, and the remanent state cannot evolve. For the case of the strain, this distinction plays no role in the physical situation since any initial stress-free strain state can be set as the reference state and identified as zero strain. However, the same change of reference state cannot be made with the polarization and electric displacement. Hence, taking the impermeable boundary conditions as an example, when the electrical boundary conditions on the crack faces are stated as $D_i n_i = 0$, this actually should be read as $\Delta D_i n_i = 0$. Furthermore, these conditions implicitly assume that a surface free charge density equal in magnitude to the remanent polarization is left on the crack faces as surfaces separate and the crack grows. If a non-zero remanent polarization is accounted for in the constitutive law and the crack face boundary conditions $D_i n_i = 0$ are applied, then such a model predicts that the electric field

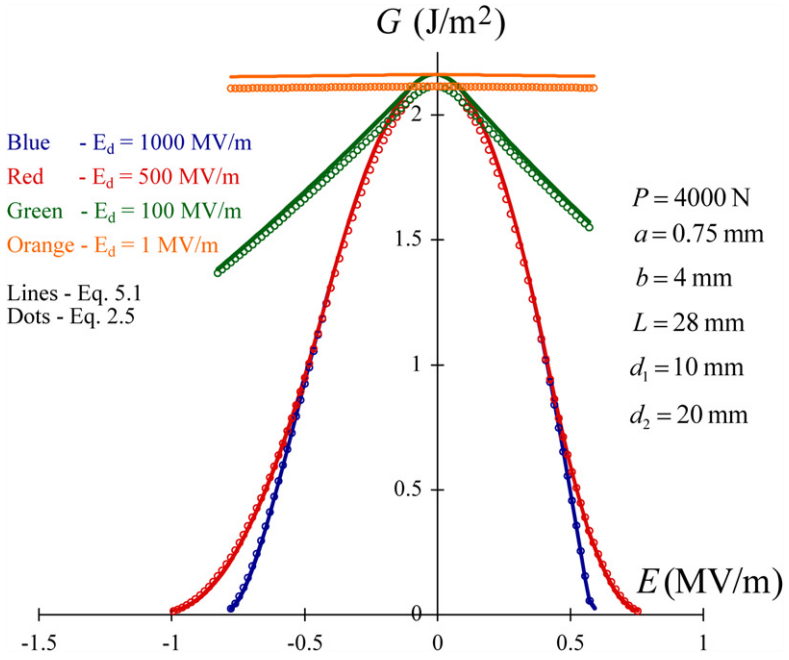

Fig. 8. The energy release rate as a function of applied electric field under a constant load using energetically consistent boundary conditions and different levels of the critical discharge field within the crack gap. Solid lines represent the results as computed from Eq. (5.1) and the dots are results computed from Eq. (2.5) using a Δa of 0.5 mm.

within the crack gap, $-\Delta\phi/\Delta u_n$, will be enormous even for zero applied electrical loading, Haug and McMeeking (2006). Even under the standard assumptions, which are more closely approximated as $\Delta D_i n_i = 0$, the electric field within the crack gap can grow to be very large for very modest applied electrical loadings. Certainly, the electric field within the crack gap cannot increase indefinitely, and eventually some type of electrical discharge will occur. A very simple model for electrical discharge (perhaps the simplest) was proposed in Eqs. (4.10) and (4.11). It is assumed that the crack gap behaves in a linear dielectric manner up to an electric field of E_d. Once this discharge field is reached, charge is allowed to transfer between the crack faces in an amount such that the electric field within the crack gap remains at E_d. We note that this idealized model for the crack gap discharge requires the vector potential finite element method for its solution. Fig. 8 illustrates the effects of electrical discharge on the energy release rate predicted using the energetically consistent boundary conditions, an applied load of 4000 N, and a crack length of 0.75 mm. Again, the lines represent the calculation of the energy release rate based on Eq. (5.1), and the dots are computed with Eq. (2.5) using a Δa of 0.5 mm. These calculations indicate that, to within numerical discretization error, the crack tip and "global" procedures for computing the energy release rate are in agreement for the energetically consistent boundary conditions. Of greater interest is the effect of the electrical discharge. Notice that as the critical electric field level for discharge E_d decreases, the effects of the applied electric field are diminished and the energy release rate increases. In the limit as $E_d \to 0$ the results for the permeable crack face boundary conditions are recovered. Therefore, when the dielectric strength of the crack gap medium is low, it becomes reasonable to apply the electrically permeable crack assumption to the fracture problem.

7. Discussion

To date there remains controversy over the appropriate electromechanical fracture criteria for piezoelectric and ferroelectric materials. The development of a mature understanding of electromechanical fracture has been hindered by a number of complex and coupled processes that are both difficult to model and measure. These processes include the effects of domain switching, electrical discharge, and the material separation process at the crack tip. There exist several excellent studies concerning the levels of electromechanical loading required to propagate cracks in

different electromechanical materials, but to date no experimental measurements have been carried out to directly measure the energy release rate for a given sample geometry and loading. Hence, the development of fracture criteria have relied on various modeling efforts to predict the prevailing energetics when fracture proceeds. On this situation, one point should be made clear; the prediction of the energy release rate is very sensitive to the assumptions about the crack face boundary conditions. This fact is illustrated in Section 6 of this paper for the specific example of the 4-point bend specimen. Instead of relying on the creativity of the modelers, a more robust approach would be to measure the energy release rates directly so that the unreasonable models can be debunked. The purpose of Section 2 of this paper is to outline the measurements that need to be performed in such an experiment. Specifically, the load-displacement and charge–voltage response of two specimens that differ in their crack lengths must be measured, and then the energy release rate for that geometry and environment can be determined. While this procedure is simple in principle, it is likely to be difficult to carry out in practice due to complications of establishing an electrical datum for the charge in the measurements, leakage currents in the circuitry, and the migration of charges from the surroundings to the sample surface. However, the outcome associated with the successful solution of these challenges would be a definitive and undeniable experimental measurement of the energy release rate in an electromechanically mixed-mode setting. Such a result would be of considerable value to the community.

The remainder of the paper was devoted to comparing the predictions for the stress and electric displacement intensity factors and energy release rates from the different crack face boundary conditions; permeable, impermeable, "exact" and energetically consistent. The results clearly show that the crack face boundary conditions significantly affect the predictions for the influence of the applied electric field on the energy release rate and the stress and electric displacement intensity factors. Furthermore, the crack tip energy release rate differs from the global energy release rate when the "exact" boundary conditions are used. This result is entirely unsatisfactory since these two quantities must be equal to one another when there is no dissipation in the system. Therefore, the only reasonable conclusion is that future modeling efforts must abandon the use of such energetically inconsistent boundary conditions in favor of energetically correct ones.

Finally, the effects of dielectric breakdown within the crack gap were investigated within the context of the energetically consistent boundary conditions. Dielectric breakdown inside cracks has been observed in fracture experiments, Schneider (2006), but not studied in detail. Hence, an understanding of the effects of discharge on fracture is not yet established. In this paper a simple model for dielectric breakdown in the crack gap was applied and it was shown that as the breakdown strength of the gap decreases, the predictions of the energetically consistent boundary conditions approach those of the permeable boundary conditions. This is a very appealing result since it offers a physical explanation for how the crack can be open but the effects of the applied electric field on the energy release rate can be greatly (or almost entirely) diminished.

Acknowledgement

WL and CML would like to acknowledge support for this work from the National Science Foundation through grant number CMS-0238522. RMM was supported by a grant from the UC Discovery Program.

Appendix A. Finite element methods

A.1. Nodal stiffness matrix condensation to the crack faces

When the crack face boundary conditions are linear, e.g. for the permeable and impermeable boundary conditions, then for each geometry only two load cases need to be solved, one mechanical and one electrical, and the solution to any other loading situation can be obtained from linear superposition. However, the "exact" and energetically consistent boundary conditions introduce non-linearity into the solution, and for a given geometry a full solution is required for each loading scenario. Since the bulk material is described by linear piezoelectricity it is very costly and unnecessary to include the nodal degrees of freedom from this region in every non-linear solution step. Hence, in order to reduce the model size and computation time, a condensation technique can be used such that only the nodal degrees of freedom associated with the opening displacement and electric potential or vector potential on the crack faces are included in the non-linear solution procedure. The condensation method is described here.

Both the standard scalar potential, Allik and Hughes (1970), and the vector potential, Landis (2002), finite element formulations can be written as

$$[K]\{u\} = \{F\}. \tag{A.1}$$

Here $[K]$ represents the global nodal stiffness matrix, $\{u\}$ represents the generalized displacement vector including both electrical and mechanical degrees of freedom, and $\{F\}$ is the generalized force applied to the body. Next we decompose the global stiffness matrix $[K]$, the displacement vector $\{u\}$, and the applied force vector $\{F\}$ in the following manner,

$$[K] = \begin{bmatrix} [K^{\mathrm{nc}}] & [C] \\ [C^{\mathrm{T}}] & [K^{\mathrm{c}}] \end{bmatrix}, \quad \{u\} = \begin{Bmatrix} u^{\mathrm{nc}} \\ u^{\mathrm{c}} \end{Bmatrix}, \quad \{F\} = \begin{Bmatrix} F^{\mathrm{nc}} \\ F^{\mathrm{c}} \end{Bmatrix}. \tag{A.2}$$

Here the superscript $^{\mathrm{nc}}$ represents the degrees of freedom that are *not* on the *crack* faces, and superscript $^{\mathrm{c}}$ represents the degrees of freedom that are on the *crack* faces. Note that in either the scalar or vector potential formulations the stiffness matrix is symmetric.

Eq. (A.1) becomes

$$\begin{bmatrix} [K^{\mathrm{nc}}] & [C] \\ [C^{\mathrm{T}}] & [K^{\mathrm{c}}] \end{bmatrix} \begin{Bmatrix} u^{\mathrm{nc}} \\ u^{\mathrm{c}} \end{Bmatrix} = \begin{Bmatrix} F^{\mathrm{nc}} \\ F^{\mathrm{c}} \end{Bmatrix}. \tag{A.3}$$

After matrix manipulation, the non-crack face degrees of freedom can be given in terms of the crack face degrees of freedom as

$$\{u^{\mathrm{nc}}\} = [K^{\mathrm{nc}}]^{-1}\{F^{\mathrm{nc}}\} - [K^{\mathrm{nc}}]^{-1}[C]\{u^{\mathrm{c}}\}. \tag{A.4}$$

Note that the only non-linearity in the problem arises from the crack face boundary conditions, which are represented by the vector $\{F^{\mathrm{c}}\}$. Hence, the inversion of the matrix $[K^{\mathrm{nc}}]$ and its operation on $[C]$ need to be performed only once and can then be stored. Using (A.4), Eq. (A.3) can now be written as

$$\underbrace{([K^{\mathrm{c}}] - [C]^{\mathrm{T}}[K^{\mathrm{nc}}]^{-1}[C])}_{[K^{\mathrm{crack}}]}\{u^{\mathrm{c}}\} = \underbrace{\{F^{\mathrm{c}}\} - [C]^{\mathrm{T}}[K^{\mathrm{nc}}]^{-1}\{F^{\mathrm{nc}}\}}_{\{F^{\mathrm{crack}}\}}. \tag{A.5}$$

Here, $[K^{\mathrm{crack}}]$ is the condensed stiffness matrix. Again, note that non-linearity enters the problem through $\{F^{\mathrm{c}}\}$. A Newton–Raphson method will be implemented to solve the problem, and this technique will introduce additional terms into the condensed Jacobian matrix. Hence, it is not useful to invert the condensed stiffness yet, but it is useful to store this matrix after one evaluation of the $[C]^{\mathrm{T}}[K^{\mathrm{nc}}]^{-1}[C]$ term.

A.2. Construction of the Jacobian matrix associated with $\{F^{\mathrm{c}}\}$

In order to simplify the presentation here we will assume a symmetric loading configuration such that the crack lies along the x-axis and the displacement and electric potential along the crack faces satisfies $u_y^- = -u_y^+$ and $\phi^- = -\phi^+$. For this type of symmetry $\Delta u_n = 2u_y^+$ and $\Delta\phi = 2\phi^+$. The formulas to be presented in this section can be readily generalized to the non-symmetric cases. We begin with the scalar potential formulation. The nodal forces normal to the crack face and the nodal charges on the crack face are arranged into the vector $\{F^{\phi}\}$, where the superscript $^{\phi}$ signifies the generalized forces associated with the scalar potential formulation. These forces can be calculated as

$$\{F^{\phi}\} = \int_S [N]^{\mathrm{T}} \begin{Bmatrix} t_y \\ -\omega \end{Bmatrix} dS \tag{A.6}$$

where t_y is the normal traction on the top crack face and ω is the surface charge density on the top crack face. The array $[N]$ is a collection of the appropriate interpolation functions associated with the nodes along the crack face. For both the "exact" and energetically consistent boundary conditions the traction and surface charge density are dependent on the crack opening displacement and electric potential drop in a non-linear fashion. For a Newton–Raphson solution

procedure the incremental relationships between the generalized nodal forces and generalized nodal displacements are required. The incremental forces can be written as

$$\{\delta F^{\phi}\} = \int_S [N]^{\mathrm{T}} \begin{Bmatrix} \delta t_y \\ -\delta\omega \end{Bmatrix} dS = \int_S [N]^{\mathrm{T}} \underbrace{\begin{bmatrix} \frac{\partial t_y}{\partial u_y} & \frac{\partial t_y}{\partial \phi} \\ -\frac{\partial \omega}{\partial u_y} & -\frac{\partial \omega}{\partial \phi} \end{bmatrix}}_{[J_\phi]} [N]\, dS \begin{Bmatrix} \delta \bar{u}_y \\ \delta \bar{\phi} \end{Bmatrix}. \tag{A.7}$$

Here, the vector $\{\delta \bar{u}_y \quad \delta \bar{\phi}\}$ is intended to represent the nodal opening displacements and electric potentials on the top crack face. The crack gap Jacobian matrices for the "exact" and energetically consistent (EC) boundary conditions are

$$[J_\phi^{\mathrm{Exact}}] = \begin{bmatrix} 0 & 0 \\ -\frac{\Delta\phi}{\Delta u_y^2}\kappa_0 & \frac{1}{\Delta u_y}\kappa_0 \end{bmatrix} \quad \text{and} \quad [J_\phi^{\mathrm{EC}}] = \begin{bmatrix} -\frac{\Delta\phi^2}{\Delta u_y^3}\frac{d^2 h_c}{dE_c^2} & \frac{\Delta\phi}{\Delta u_y^2}\frac{d^2 h_c}{dE_c^2} \\ \frac{\Delta\phi}{\Delta u_y^2}\frac{d^2 h_c}{dE_c^2} & -\frac{1}{\Delta u_y}\frac{d^2 h_c}{dE_c^2} \end{bmatrix}. \tag{A.8}$$

Note that the crack gap Jacobian and hence the full finite element Jacobian is symmetric for the energetically consistent boundary conditions but not symmetric for the "exact" boundary conditions.

We now present the analogous matrices for the vector potential formulation. The generalized nodal forces for the vector potential formulation are given as

$$\{F^{\psi}\} = \begin{Bmatrix} \int_S [N]^{\mathrm{T}} t_y\, dS \\ -\int_S [B]^{\mathrm{T}} \phi n_y\, dS \end{Bmatrix} \tag{A.9}$$

Here, $[N]$ are the appropriate shape functions associated with the crack surface, and $[B]$ are the derivatives of the shape functions with respect to the direction of the crack face. In a manner analogous to Eq. (A.7) the increments of the generalized forces for the vector potential formulation can be written as

$$\{\delta F^{\psi}\} = \int_S [\bar{N}]^{\mathrm{T}} [J_\psi] [\bar{N}]\, dS \begin{Bmatrix} \delta \bar{u}_y \\ \delta \bar{\psi} \end{Bmatrix} \quad \text{with } [\bar{N}] = \begin{bmatrix} [N] & [0] \\ [0] & [B] \end{bmatrix} \tag{A.10}$$

where the crack gap Jacobian matrices for the "exact" and energetically consistent boundary conditions are

$$[J_\psi^{\mathrm{Exact}}] = \begin{bmatrix} 0 & 0 \\ \frac{D_c}{\kappa_0} & -\frac{u_y}{\kappa_0} \end{bmatrix} \quad \text{and} \quad [J_\psi^{\mathrm{EC}}] = \begin{bmatrix} 0 & E_c \\ E_c & -\frac{d^2 \tilde{u}_c}{dD_c^2} u_y \end{bmatrix}. \tag{A.11}$$

Again notice that the crack gap Jacobian for the energetically consistent boundary conditions is symmetric but that for the "exact" boundary conditions is not. Also, for the vector potential formulation it is more useful to use the internal energy of the crack $\tilde{u}_c(D_c) = h_c + E_c D_c$, which is a function of the electric displacement within the gap. Then the electric field within the crack is simply $E_c = d\tilde{u}_c/dD_c$ and the traction on the crack surfaces is $\sigma_c = \tilde{u}_c$.

Using the finite element Jacobian matrices for the crack faces defined here, Eq. (A.5) can be solved using a standard Newton–Raphson method. Again, the Newton–Raphson Jacobian matrix will be symmetric for the energetically consistent boundary conditions, but not for the "exact" boundary conditions. Due to the condensation step, the matrix to be inverted at each Newton–Raphson iteration is fully dense but is only the size of twice the number of nodes on the crack face (for symmetric 2-D simulations). This reduction in the system size allows for relatively rapid computation which is very useful for the investigation of many different loading scenarios on a given crack geometry.

Appendix B

The material properties used for numerical results are characteristic of PIC-151, Heyer et al. (1998).

The Irwin matrix for this material under plane strain conditions is

$$\begin{bmatrix} H_{11} & H_{12} \\ H_{21} & H_{22} \end{bmatrix} = \begin{bmatrix} 1.119 \times 10^{-11}\ \mathrm{m^2/N} & 9.901 \times 10^{-3}\ \mathrm{m^2/C} \\ 9.901 \times 10^{-3}\ \mathrm{m^2/C} & -3.110 \times 10^{7}\ \mathrm{V\,m/C} \end{bmatrix}$$

where the plane strain material properties used to derive this matrix are in h-form:

$$c_{11}^D = 122\ \mathrm{GPa}, \qquad c_{13}^D = 44.8\ \mathrm{GPa}, \qquad c_{33}^D = 130.2\ \mathrm{GPa}, \qquad c_{44}^D = 34.7\ \mathrm{GPa},$$
$$h_{31} = -1.27 \times 10^9\ \mathrm{V/m}, \qquad h_{33} = 2.00 \times 10^9\ \mathrm{V/m}, \qquad h_{15} = 1.22 \times 10^9\ \mathrm{V/m},$$
$$\beta_{11}^{\varepsilon} = 1.108 \times 10^8\ \mathrm{V\,m/C}, \qquad \beta_{33}^{\varepsilon} = 1.326 \times 10^8\ \mathrm{V\,m/C}$$

or in e-form

$$c_{11}^E = 110 \times 10^9 \text{ N/m}^2, \qquad c_{13}^E = 64 \times 10^9 \text{ N/m}^2,$$
$$c_{33}^E = 100 \times 10^9 \text{ N/m}^2, \qquad c_{44}^E = 20 \times 10^9 \text{ N/m}^2,$$
$$e_{31} = -9.6 \text{ C/m}^2, \qquad e_{33} = 15.1 \text{ C/m}^2, \qquad e_{15} = 12 \text{ C/m}^2,$$
$$\kappa_{11}^\varepsilon = 98.24 \times 10^{-10} \text{ C/V m}, \qquad \kappa_{33}^\varepsilon = 75.3 \times 10^{-10} \text{ C/V m}.$$

References

Allik, H., Hughes, T.J.R., 1970. Finite element method for piezoelectric vibration. Int. J. Numer. Methods Engrg. 2, 151–157.

Anderson, T.L., 1991. Fracture Mechanics Fundamental and Applications. CRC Press, Boca Raton, FL.

Deeg, W.F., 1980. The analysis of dislocation, crack and inclusion problems in piezoelectric solids. PH.D. Thesis, Stanford University.

Dunn, M.L., 1994. The effects of crack face boundary conditions on the fracture mechanics of piezoelectric solids. Engrg. Fract. Mech. 48, 25–39.

Hao, T.H., Shen, Z.Y., 1994. A new electric boundary condition of electric fracture mechanics and its application. Engrg. Fract. Mech. 47, 793–802.

Haug, A., McMeeking, R.M., 2006. Cracks with surface charge in poled ferroelectrics. Eur. J. Mech. A Solids 25, 24–42.

Heyer, V., Schneider, G.A., Balke, H., Drescher, J., Bahr, H.A., 1998. A fracture criterion for conducting cracks in homogeneously poled piezoelectric PZT-PIC 151 ceramics. Acta Mat. 46, 6615–6622.

Landis, C.M., 2002. A new finite element formulation for electromechanical boundary value problems. Int. J. Numer. Methods Engrg. 55, 613–628.

Landis, C.M., 2004. Energetically consistent boundary conditions for electromechanical fracture. Int. J. Solids Struct. 41, 6291–6315.

Li, F.Z., Shih, C.F., Needleman, A., 1985. A comparison of methods for calculating energy release rates. Engrg. Fract. Mech. 21 (2), 405–421.

Li, W., 2006. On the crack face boundary conditions in electromechanical fracture and an experimental protocol for determining energy release rates, Master's Thesis, Rice University.

McMeeking, R.M., 1999. Crack tip energy release rate for a piezoelectric compact tension specimen. Engrg. Fract. Mech. 64, 217–244.

McMeeking, R.M., 2004. The energy release rate for a Griffith crack in a piezoelectric material. Engrg. Fract. Mech. 71, 1149–1163.

Pak, Y.E., 1992. Linear electro-elastic fracture mechanics of piezoelectric materials. Int. J. Fract. 54, 79–100.

Parks, D.M., 1974. A stiffness derivative finite element technique for determination of crack tip stress intensity factors. Int. J. Fract. 10 (4), 487–502.

Parton, V.Z., 1976. Fracture mechanics of piezoelectric materials. Acta Astronaut. 3, 671–683.

Schneider, G., 2006. Private communications.

Suo, Z., Kuo, C.M., Barnett, D.M., Willis, J.R., 1992. Fracture mechanics for piezoelectric ceramics. J. Mech. Phys. Solids 40, 739–765.